Thermal-hydraulic analysis of the DTT Toroidal Field magnets in DC operation

Thermal-Hydraulic Analysis of the DTT Toroidal Field Magnets in DC Operation

R. Bonifetto, *Associate Member, IEEE*, A. Di Zenobio, L. Muzzi, *Member, IEEE*, S. Turtù, *Member, IEEE*, R. Zanino, *Senior Member, IEEE*, and A. Zappatore, *Associate Member, IEEE*, and DTT design contributors

***Abstract*—The Divertor Tokamak Test (DTT) facility is currently under design in Italy. This fully superconductive compact tokamak will be the test bench of several DEMO-relevant divertor solutions.**

The 4C code model of a DTT toroidal field magnet (including its structures) is developed here and used to support some important design decisions related to the neutron shield to be adopted, the need of an active cooling of the casing and the static heat load reduction.

The simulations confirm the need to actively cool the casing by suitable cooling channels, but also the need of a proper neutron shield to reduce the nuclear heat load on the superconducting coils. On the other hand, the proposed static heat load reduction measures do not appear to be effective enough to satisfy the design requirement of 1.4 K for the minimum temperature margin.

***Index Terms*—- DTT, modeling, nuclear fusion, thermal-hydraulics, toroidal field magnet**

I. Introduction

In the EU DEMO fusion reactor, currently in its pre-conceptual design phase [1], the power exhaust issue associated to the long plasma pulse duration and the large thermal loads represents a dramatic challenge, so that a new, robust design of the divertor is needed. For this reason, several DEMO-relevant divertor solutions will be tested in the Divertor Tokamak Test (DTT) facility that is going to be built in Italy [2]. The DTT will be a compact fully superconductive tokamak, with a major radius of 2.14 m and an aspect ratio of 3.3, very flexible in terms of plasma configurations [3]. The superconducting (SC) magnets will provide a toroidal magnetic field on the plasma axis of 6 T, and the plasma current will depend on the specific divertor solution and can be as high as 5.5 MA [2].

The 18 Toroidal Field (TF) magnets, cooled in parallel by forced-flow supercritical helium at 4.5 K, and carrying a nominal current of 44.8 kA, must then be reliable components, capable to cope with several different operating scenarios.

The 4C code [4], aimed at the analysis of thermal-hydraulic transients in superconducting magnets and recently validated also in predictive mode [5], is used here to develop a detailed model of the ~5 m tall DTT TF magnet, including both the winding pack (WP) and the casing. The model is applied to assess the impact of different design options for the neutronic and thermal shield (TS) on the TF magnet performance in DC (direct current) operating mode, namely during the plasma (pulsed) operation.

II. The DTT TF Magnet and Its 4C Model

After a first design featuring a mixed layer/pancake winding [6], the current WP design is based on a pancake winding of rectangular, Nb_3Sn Cable-in-Conduit Conductors (CICCs), Fig. 1a. The DTT TF CICCs are geometrically similar to those of the JT-60SA TF coils [7] and they do not feature any channel with low hydraulic impedance (as the maximum length of a single hydraulic channel is ~110 m).

The winding is made of five double-pancakes (DPs), with the 10 resulting pancakes (Ps) cooled in parallel by forced-flow supercritical He (SHe) at 6 bar and 4.5 K. The hydraulic inlets are located close to the gravity support (GS) region (see Fig. 2), at the inner side of the coil, where the magnetic field and the nuclear heat load coming from the plasma reactions reach their peak, in order to provide the freshest He and thus the most effective cooling to the first turns. As both the internal joints and the coil terminations are located at the outer coil radius, the SHe is supplied at the conductor mid-length (one inlet for each DP): as shown in Fig. 1b, this results in counter-current flow in adjacent Ps (see the different direction of the SHe flow in the odd and even Ps in Fig. 2).

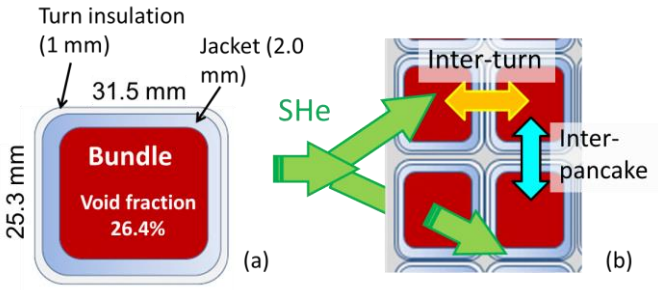

Fig. 1 (a) Cross section of the DTT TF conductor and (b) sketch of the inter-turn and inter-pancake thermal coupling paths accounted for by the 4C WP model. The location of the common inlet of each double pancake, at the coil bore, is also shown, resulting in a counterflow of the SHe in adjacent pancakes.

Manuscript receipt and acceptance dates will be inserted here. *(Corresponding author: Roberto Bonifetto.)*

R. Bonifetto, R. Zanino and A. Zappatore are with the NEMO Group, Dipartimento Energia, Politecnico di Torino, Torino 10124, Italy (e-mail: roberto.bonifetto@polito.it; roberto.zanino@polito.it; andrea.zappatore@polito.it).

A. Di Zenobio, L. Muzzi and S. Turtù are with ENEA, Superconductivity Section, C.R. Frascati, Frascati 00044, Italy.

Color versions of one or more of the figures in this paper are available online at http://ieeexplore.ieee.org.

Digital Object Identifier will be inserted here upon acceptance.

The Darcy-Forcheimer friction factor correlation for the flow in porous media [8] is used to compute the pressure drop in the CICC, as it accurately predicts the friction in the (similar) JT-60SA conductor. As a result, for a prescribed pressure drop of ~1 bar, a SHe mass flow rate of ~2.5 g/s in each hydraulic channel is computed.

The thermal coupling between neighboring turns and Ps of the WP is accounted for, as shown in Fig. 1b, including the thermal resistance provided by the 1 mm turn insulation (and 0.5 mm DP insulation where relevant). The nominal value of this (temperature dependent) thermal resistance has been increased by a factor 5 to account for the multi-layer nature of the turn and DP insulation, as already done when calibrating the same resistance using experimental data from other similar WPs (JT-60SA central solenoid [9], KSTAR PF coils [10]). The increase of a factor 5 with respect to the nominal value has a small impact (~10 mK) on the minimum temperature margin (ΔT_{marg}^{min}); the case with reduced thermal coupling presented here is more conservative, in view of the reduced contribution of the successive turns to the cooling of the first one, where the ΔT_{marg}^{min} is located. However, further parametric analyses on this multiplier are envisaged to better assess the dependence of the results on this parameter.

The SC scaling parameters adopted for the DTT TF conductor in the critical current scaling law [11] are reported in Table I.

The WP, wrapped in 6 mm of ground insulation, is encapsulated in a bulky stainless-steel casing capable to withstand the Lorentz forces acting on the coil during operation. The entire magnet is mechanically supported by the GS, laying on the pedestal ring (see Fig. 2).

TABLE I
Nb_3Sn CONDUCTOR SCALING PARAMETERS

Parameter	Value
C_0	86765 [A×T/mm^2]
B_{c20m}	32.97 [T]
T_{c0m}	16.06 [K]
C_{a1}	44.48
C_{a2}	0
ε_{0a}	0.256e−2
ε_m	−4.9e−4
p	0.63
q	2.1
Conductor *n*-value	6
Effective strain	−0.65%

In the model, the coil structures are discretized poloidally in 16, 2D radial-toroidal cross sections (cuts) following the same discretization adopted in the Monte Carlo neutronic simulations used to evaluate the nuclear heat load on the magnet [12]. A view of the two equatorial cuts is reported in Fig. 3, showing also the nuclear heat load distribution on the same cuts for case C (see Section III.A). The 2D heat conduction equation is solved on each cut, thermally coupled with the WP except on the plasma-facing side: during operation, indeed, the Lorentz forces on the WP push it outwards, detaching it from the casing. That side of the WP is thus considered adiabatic in the simulations (when the coil is charged).

One of the TF magnet design options foresees an active cooling of the casing, independent from the WP one, provided by 4 casing cooling channels (CCCs), supplied in parallel by SHe at 6 bar and 4.5 K. They feature a circular steel pipe inserted in 4 grooves machined in the side wall of the casing, see the black circles in Fig. 3.

The evolution of the SHe velocity, pressure and temperature distributions along the CCCs axis is also computed by the 4C model.

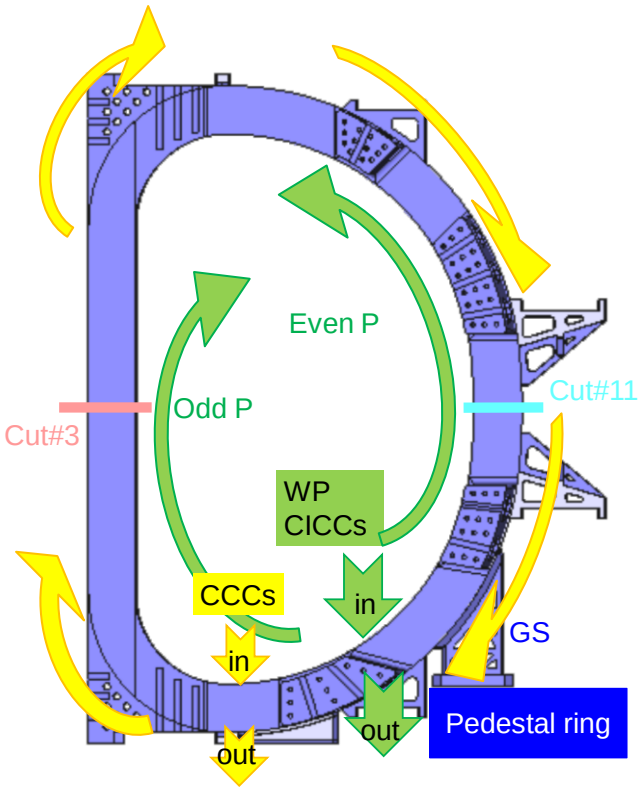

Fig. 2 Side view of a DTT TF coil. The SHe inlets/outlets and flow directions are shown by the arrows for both WP and casing cooling channels (green and yellow, respectively). The location of the two (inboard and outboard) equatorial cuts, out of the 16 in total, used to poloidally discretize the casing are shown in pink and cyan, respectively. The location of the gravity support (GS) and of the pedestal ring is also shown.

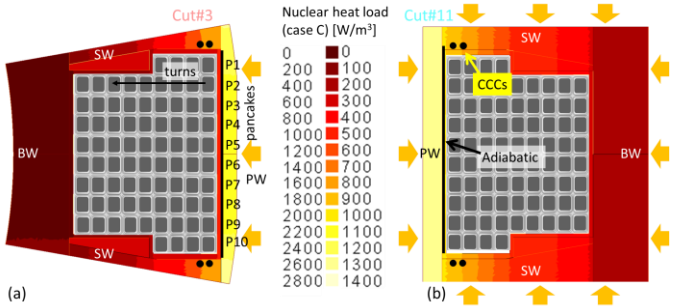

Fig. 3 View of the radial-toroidal equatorial inboard (a) and outboard (b) cross sections used to poloidally discretize the TF coil casing. The 2D color map shows the distribution of the nuclear heat load [12] for case C, see Section III.A, while the orange arrows indicate the sides experiencing radiative heat load from the TS. The location of the 4 CCCs is shown by the black circles, while the black line indicates the adiabatic side of the WP with respect to the casing. The numbering of the pancakes adopted in this work is also shown. (PW = plasma wall, SW = side wall, BW = back wall.)

III. Effect of Some Parameters on the Temperature Margin in Normal Operation

A. Simulation Setup

The DTT reference plasma scenarios, namely the Single Null (SN) and Double Null (DN), are shown in Fig. 4. The time between two pulses is ~1 h, while the maximum plasma duration is foreseen to be ~52 (67) s in the SN (DN). For this reason, in order to assess the performance of the TF in the most conservative scenario, only the DN is simulated here.

The coil casing is subject to:

- Static radiative heat load from the TS, cooled by gaseous He entering at 80 K;
- Static conductive heat load from the pedestal ring (also kept at ~80 K) to the coil through the GS.

The former heat load is applied to all surfaces facing the TS (conservatively considered to be kept at 100 K, as the pedestal ring, because the inlet temperature is ~80 K and the target outlet temperature is ~100 K [2], and with an emissivity of 0.15 [2]), namely all the surfaces of the outboard leg (see the orange arrows in Fig. 3b) and the plasma-facing surface of the inboard leg (see Fig. 3a). The other three surfaces of the inboard leg face either other TF coils or the central solenoid, actively cooled by SHe at 4.5 K, so that they can be considered adiabatic. As a result, the computed static radiative load on 18 TF coils turns out to be ~0.3 kW, while the conductive heat load ~0.1 kW.

The magnetic field distribution along the axis of three selected Ps is shown in Fig. 5a. It includes the contribution of all the coils and of the plasma; the field gradient on the cable cross section is also accounted for in the calculation of the current sharing temperature, used to evaluate the temperature margin.

The 1D map of the nuclear heat load on the same selected Ps is also reported in Fig. 5b [12]: it is computed by Monte Carlo simulations already including a safety factor of 1.5, and has a peak at 1.5 W/m (corresponding to ~2 mW/cm^3). In the even Ps the maximum magnetic field and nuclear heat load are reached at a longer distance from the SHe inlet than in the odd Ps, because in the former ones the SHe has to travel a longer path before reaching the inboard equatorial cut, experiencing the peak values, see Fig. 2.

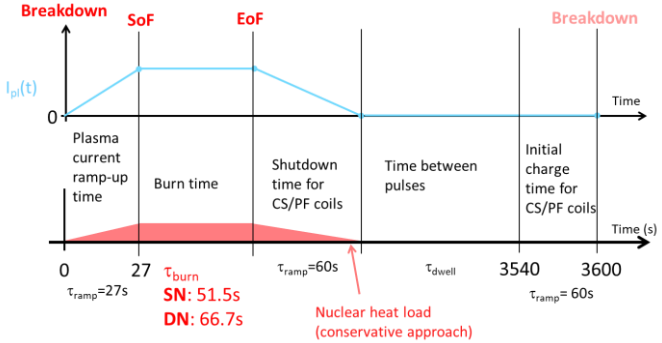

Fig. 4 DTT reference plasma scenarios (Single Null, SN, and Double Null, DN). The top part reports the plasma current qualitative behavior, while the nuclear heat load on the TF coils is shown in the bottom part. The time axis is not to scale. (SoF = start of plasma current flat-top, EoF = end of plasma current flat-top.)

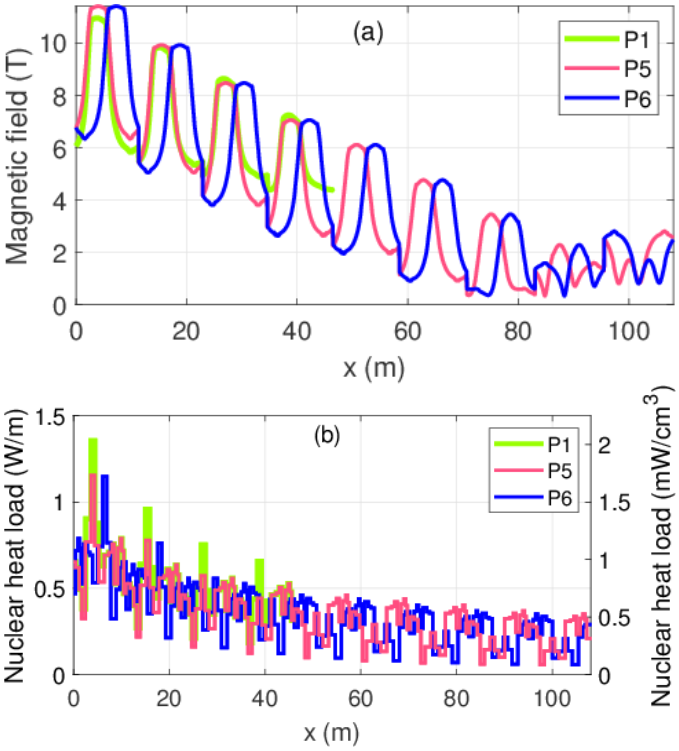

Fig. 5 Magnetic field (a) and nuclear heat load [12] (b) distribution in 3 reference pancakes (namely, side pancake P1 and the two central pancakes P5 and P6).

Two different design options (plus a limiting case) are foreseen for the neutron shield, namely:

- Case A, with welding of the shield in correspondence of the TF coil boundaries, see Fig. 6a (the welding locations are weak points from the shielding point of view, as they break the continuity of the shield);
- Case B, thinner shield with welding in the middle of the WP;
- Case C (limiting case): no neutron shield, considered here of course just for the sake of this parametric study.

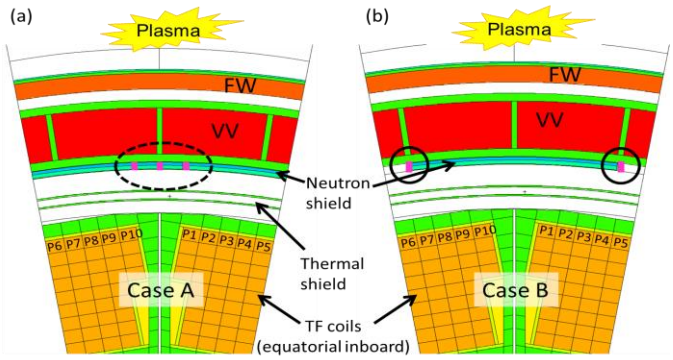

Fig. 6 Different design options of the neutron shield [12]: (a) case A, with three welding (purple in the black dashed ellipse) between two neighboring TF coils; (b) case B with one welding in the middle of the WP (purple in the black circles). (FW = first wall, VV = vacuum vessel.)

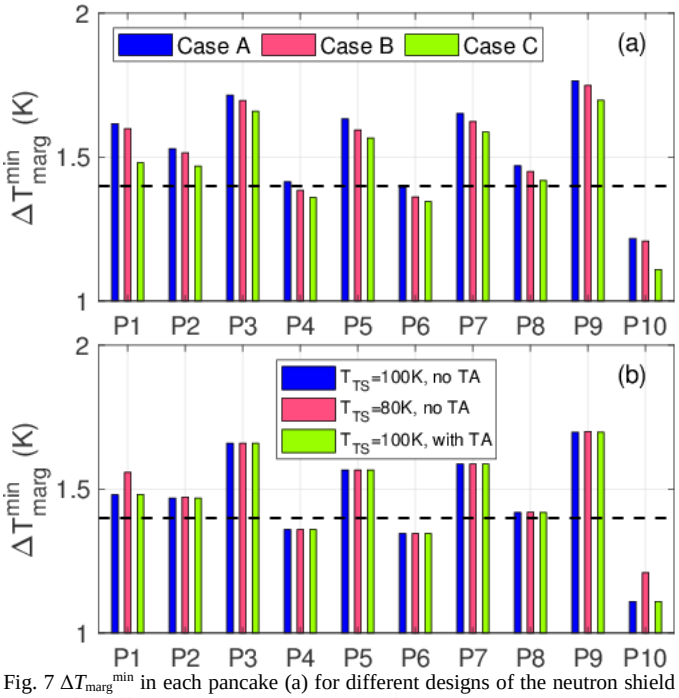

Fig. 7 ΔT_{marg}^{min} in each pancake (a) for different designs of the neutron shield and (b) for different operating temperatures of the TS or with a thermal anchor (TA) at 40 K on the GS, for case C. The horizontal dashed black line indicates the design value of the ΔT_{marg}^{min}. All the results are without CCCs.

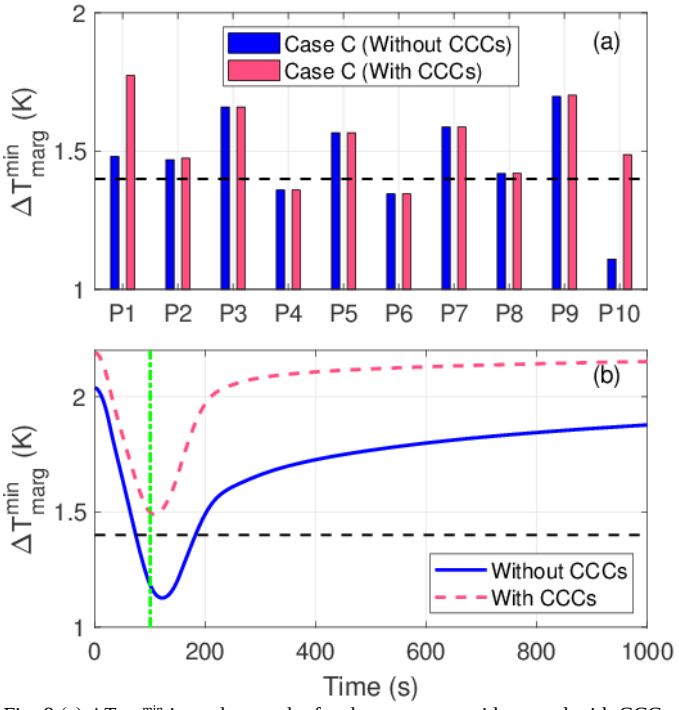

Fig. 8 (a) ΔT_{marg}^{min} in each pancake for the two cases without and with CCCs. (b) Evolution of the ΔT_{marg}^{min} in P10 for the same two design options during the first 1000 s of the periodic pulse. The horizontal dashed black line indicates the design value of the ΔT_{marg}^{min}, while in (b) the vertical dash-dotted green line corresponds to the EoF. All the results are for case C.

B. *Results*

The ΔT_{marg}^{min} adopted as a target during the design is 1.4 K [2]. The results comparing the performance (in terms of ΔT_{marg}^{min} in each P) among the different neutron shield designs are shown in Fig. 7, for the case without active cooling of the casing (no CCCs). As expected, case A provides the best shielding of the WP (it is the only case for which at least all the central Ps satisfy the design constraint $\Delta T_{marg}^{min} > 1.4$ K), while case B shows in general a ΔT_{marg}^{min} reduction of few tens of mK, especially in the central Ps. The worst performance is obviously shown by case C. However, in all cases in P10 $\Delta T_{marg}^{min} < 1.4$ K, asking for the implementation of an active cooling of the casing. The difference between case A and case B is small, always < 0.1 K: the details of the shield design are not that dramatically important.

The ΔT_{marg}^{min} difference in odd and even pancakes is due to the above-mentioned different length run by the SHe before reaching the peak field and nuclear heat load region (see P5 and P6 in Fig. 5), leading to a different accumulated heat load.

Some possible alternatives to the active cooling of the casing are also investigated, in the limiting case C, such as the reduction of the TS temperature to maximum 80 K or the installation of a thermal anchor (TA) at 40 K on the GS (of course this will lead to a higher refrigeration cost, to be carefully assessed). As reported in Fig. 7b, the latter measure is ineffective, while the former can increase the ΔT_{marg}^{min} of only ~0.1 K on the side Ps (the central Ps are not affected because they are detached from the casing, so their ΔT_{marg}^{min} does not depend on the casing temperature), which is however not sufficient.

On the other hand, as reported in Fig. 8a, the use of CCCs to actively cool the casing can reduce the heating of the side Ps from casing, increasing the ΔT_{marg}^{min} above the design threshold (without the need to reduce the TS temperature). In order to have the same constraint satisfied also by the central Ps, however, the use of a neutron shield is needed.

The evolution of the ΔT_{marg}^{min} in P10 for the cases without and with CCCs (case C) is also shown in Fig. 8b. The ΔT_{marg}^{min} is reached after the EoF, during the plasma shut down; when the casing is actively cooled, the WP cooling dynamics is faster and the ΔT_{marg}^{min} suddenly starts to increase after the EoF. On the contrary, if the WP cooling He should take care also of the heat load deposited in the casing (not actively cooled), it will take some tens of seconds longer for the CICC recooling to be effective (and for the ΔT_{marg}^{min} to start increasing again).

IV. Conclusions and Perspective

The 4C model of a DTT toroidal field magnet has been developed, including also its structures and their cooling.

The model has been applied to investigate the effects on the performance in DC (direct current) operation of different design options for the neutron shield, the casing cooling, the operating temperature of the thermal shield and the gravity support thermal anchor.

The neutron shield and the casing cooling channels are both needed to fulfill the 1.4 K minimum temperature margin requirement prescribed during the design, while reducing the

thermal shield temperature (and thus the radiative heat load) alone is not sufficient.

In perspective, the same model will be used to further support the DTT magnet design analyzing other relevant transients (e.g. cooldown, plasma disruption, quench, fast current discharge).

REFERENCES

[1] G. Federici et al., "DEMO design activity in Europe: progress and updates," *Fus. Eng. Des.*, vol. 136, 2018, pp. 729–741.

[2] ENEA Frascati Research Center, Italy. DTT Divertor Tokamak Test facility Interim Design Report April 2019 [Online]. Available: https://www.dtt-project.enea.it/downloads/DTT_IDR_2019_WEB.pdf, Accessed on Sep. 23, 2019.

[3] G.M. Polli, "Divertor Tokamak Test facility Plant Integration Document (PID)" v1.3, May 24, 2019.

[4] L. Savoldi Richard, F. Casella, B. Fiori, and R. Zanino, "The 4C code for the cryogenic circuit conductor and coil modeling in ITER," *Cryogenics*, vol. 50, 2010, pp. 167–176.

[5] R. Zanino, R. Bonifetto, A. Brighenti, T. Isono, H. Ozeki, and L. Savoldi, "Prediction, experimental results and analysis of the ITER TF Insert Coil quench propagation tests, using the 4C code," *Supercond. Sci. Technol.*, vol. 31, 2018, Art. no 035004.

[6] A. Di Zenobio et al., "DTT Device: conceptual design of the superconducting magnet system," *Fus. Eng. Des.*, vol. 122, Nov. 2017, pp. 299-312.

[7] L. Zani, P. Barabaschi, E. Di Pietro, and M. Verrecchia, "Completion of TF Strand Production and Progress of TF Conductor Manufacture for JT-60SA Project," *IEEE Trans. Appl. Supercond.*, vol. 24, no. 3, Jun. 2014, Art. No. 6000105.

[8] M. Bagnasco, L. Bottura, and M. Lewandowska, "Friction factor correlation for CICC's based on a porous media analogy," *Cryogenics*, vol. 50, 2010, pp. 711–719.

[9] R. Bonifetto, L. Savoldi, and R. Zanino, "Thermal-hydraulic analysis of the JT-60SA Central Solenoid operation," *IEEE Trans. Appl. Supercond.*, vol. 29, no. 5, Aug. 2019, Art. no. 4201005.

[10] L. Savoldi Richard, R. Bonifetto, Y. Chu, A. Kholia, S. H. Park, H. J. Lee, and R. Zanino, "4C code analysis of thermal-hydraulic transients in the KSTAR PF1 superconducting coil," *Cryogenics*, vol. 53, Jan. 2013, pp. 37–44.

[11] L. Bottura, and B. Bordini, "Jc(B, T, ε) Parameterization for the ITER Nb3Sn production," *IEEE Trans. Appl. Supercond.*, vol. 19, no. 3, Jun. 2009, pp. 1521–1524.

[12] R. Villari, ENEA Frascati Research Center, Via E. Fermi 45, 00044 Frascati (Italy), private communication, Jul. 2019.